

Steady-state and transient lectronic transport properties of β-$(Al_x)Ga_{1-x})_2O_3/Ga_2O_3$ heterostructures: An ensemble Monte Carlo simulation

Yan Liu(刘妍), Ping Wang(王平), Ting Yang(杨婷), Qian Wu(吴茜), Yintang Yang(杨银堂), and Zhiyong Zhang(张志勇)

Citation: Chin. Phys. B, 2022, 31 (**11**): 117305. DOI: 10.1088/1674-1056/ac7290

What follows is a list of articles you may be interested in

Quantum transport signatures of non-trivial topological edge states in a ring-shaped Su-Schrieffer-Heeger double-chain system

Cheng-Zhi Ye(叶成芝), Lan-Yun Zhang(张蓝云), and Hai-Bin Xue(薛海斌)
Chin. Phys. B, 2022, 31 (**2**): 027304. DOI: 10.1088/1674-1056/ac34ff

Implementation of synaptic learning rules by TaO_x memristors embedded with silver nanoparticles

Yue Ning(宁玥), Yunfeng Lai(赖云锋), Jiandong Wan(万建栋), Shuying Cheng(程树英), Qiao Zheng(郑巧), and Jinling Yu(俞金玲)
Chin. Phys. B, 2021, 30 (**4**): 047301. DOI: 10.1088/1674-1056/abccb8

Hydrodynamic simulation of chaotic dynamics in InGaAs oscillator in terahertz region

Wei Feng(冯伟)
Chin. Phys. B, 2020, 29 (**4**): 047302. DOI: 10.1088/1674-1056/ab696f

Comparative study on transport properties of N-, P-, and As-doped SiC nanowires: Calculated based on first principles

Ya-Lin Li(李亚林), Pei Gong(龚裴), Xiao-Yong Fang(房晓勇)
Chin. Phys. B, 2020, 29 (**3**): 037304. DOI: 10.1088/1674-1056/ab6c4c

Transport spectroscopy through dopant atom array in silicon junctionless nanowire transistors

Xiao-Song Zhao(赵晓松), Wei-Hua Han(韩伟华), Yang-Yan Guo(郭仰岩), Ya-Mei Dou(窦亚梅), Fu-Hua Yang(杨富华)
Chin. Phys. B, 2018, 27 (**9**): 097310. DOI: 10.1088/1674-1056/27/9/097310

Steady-state and transient electronic transport properties of β-$(Al_xGa_{1-x})_2O_3/Ga_2O_3$ heterostructures: An ensemble Monte Carlo simulation

Yan Liu(刘妍)[1], Ping Wang(王平)[1,†], Ting Yang(杨婷)[1], Qian Wu(吴茜)[1], Yintang Yang(杨银堂)[2], and Zhiyong Zhang(张志勇)[3]

[1] *State Key Laboratory of Integrated Service Networks, School of Telecommunications Engineering, Xidian University, Xi'an* 710071, *China*
[2] *Key Laboratory of the Ministry of Education for Wide Band-Gap Semiconductor Materials and Devices, School of Microelectronics, Xidian University, Xi'an* 710071, *China*
[3] *School of Information Science and Technology, Northwest University, Xi'an* 710127, *China*

(Received 26 February 2022; revised manuscript received 19 May 2022; accepted manuscript online 24 May 2022)

The steady-state and transient electron transport properties of β-$(Al_xGa_{1-x})_2O_3/Ga_2O_3$ heterostructures were investigated by Monte Carlo simulation with the classic three-valley model. In particular, the electronic band structures were acquired by first-principles calculations, which could provide precise parameters for calculating the transport properties of the two-dimensional electron gas (2DEG), and the quantization effect was considered in the Γ valley with the five lowest subbands. Wave functions and energy eigenvalues were obtained by iteration of the Schrödinger–Poisson equations to calculate the 2DEG scattering rates with five main scattering mechanisms considered. The simulated low-field electron mobilities agree well with the experimental results, thus confirming the effectiveness of our models. The results show that the room temperature electron mobility of the β-$(Al_{0.188}Ga_{0.812})_2O_3/Ga_2O_3$ heterostructure at 10 kV·cm^{-1} is approximately 153.669 cm^2·V^{-1}·s^{-1}, and polar optical phonon scattering would have a significant impact on the mobility properties at this time. The region of negative differential mobility, overshoot of the transient electron velocity and negative diffusion coefficients are also observed when the electric field increases to the corresponding threshold value or even exceeds it. This work offers significant parameters for the β-$(Al_xGa_{1-x})_2O_3/Ga_2O_3$ heterostructure that may benefit the design of high-performance β-$(Al_xGa_{1-x})_2O_3/Ga_2O_3$ heterostructure-based devices.

Keywords: electron transport, first-principles calculations, Monte Carlo simulation

PACS: 73.40.–c, 73.63.Hs, 74.25.Jb **DOI:** 10.1088/1674-1056/ac7290

1. Introduction

As a wide band gap semiconductor, gallium oxide (Ga_2O_3) is attractive for high-power electronics and ultraviolet optoelectronic applications.[1,2] β-Ga_2O_3 has the most stable crystal structure among the five phases (α, β, γ, ε, and δ) of Ga_2O_3.[3] β-Ga_2O_3 also has excellent intrinsic material properties, including a large breakdown field strength of $\sim$ 8 MV·cm^{-1},[4] a high Baliga figure of merit of $\sim$ 3444,[5] and the availability of high-quality native substrates grown directly from the melt.[4] β-$(Al_xGa_{1-x})_2O_3$ is a ternary alloy of β-Ga_2O_3 with a tunable band gap ranging from 4.8 eV to 6 eV.[6,7] In particular β-$(Al_xGa_{1-x})_2O_3/Ga_2O_3$ heterostructures can be formed,[8] and the introduction of ternary alloys and the formation of heterostructures can significantly increase the number of possible applications and the performance of devices.[9] Knowledge about transport properties is a fundamental instrument for any physicist or engineer involved in technology design and preparation of semiconductor-based devices. Thus, the electron transport properties in β-$(Al_xGa_{1-x})_2O_3/Ga_2O_3$ heterostructures must be understood in depth. Recently, some studies have been carried out to explore the performance of β-$(Al_xGa_{1-x})_2O_3/Ga_2O_3$ heterostructures.[10–21] Zhang *et al.*[13] measured the mobilities of a modulation-doped β-$(Al_{0.18}Ga_{0.82})_2O_3/Ga_2O_3$ heterostructure grown by oxygen plasma-assisted molecular beam epitaxy as 180 cm^2·V^{-1}·s^{-1} at 300 K and 2790 cm^2·V^{-1}·s^{-1} at 90 K. Later, this group[15] fabricated a modulation-doped field effect transistor based on the β-$(Al_{0.18}Ga_{0.82})_2O_3/Ga_2O_3$ heterostructure. Their results showed that the two-dimentional electron gas (2DEG) channel mobility and saturation velocity of this device at 50 K were 1520 cm^2·V^{-1}·s^{-1} and 1.1×10^7 cm·s^{-1}, respectively. Ranga *et al.*[19] prepared modulation-doped β-$(Al_xGa_{1-x})_2O_3/Ga_2O_3$ heterostructures by metalorganic vapor-phase epitaxy. They observed that the mobility was 111 cm^2·V^{-1}·s^{-1} at room temperature. Ghosh and Singisetti[20] calculated the electron mobility by solving the Boltzmann transport equation and found that the mobility improved on the higher 2DEG density side as the remote impurity center moved away from the interface. The aforementioned investigations concerned doped β-$(Al_xGa_{1-x})_2O_3/Ga_2O_3$ heterostructures, and the electron mobility will be heavily affected by the impurity scattering because of the dopant impurities;[13,14,20] therefore, the performance of heterostructure-based devices will be seriously limited.[15,20] Actually, it is feasible to limit the carriers at the

†Corresponding author. E-mail: pingwang@xidian.edu.cn
© 2022 Chinese Physical Society and IOP Publishing Ltd

interface of unintentionally doped β-$(Al_xGa_{1-x})_2O_3$/Ga_2O_3 heterosystems owing to the staggered band alignment with a positive conduction band offset and small valence band offset between β-$(Al_xGa_{1-x})_2O_3$ and β-Ga_2O_3. Free carriers would be transferred to the high-purity β-Ga_2O_3 layer where they could populate a narrow potential well and form a high-density 2DEG. This phenomenon has also been observed in the unintentionally doped AlGaAs/GaAs heterostructures,[22] which are similar to β-$(Al_xGa_{1-x})_2O_3$/Ga_2O_3 heterostructures.[11] Moreover, the unintentionally doped heterostructures can be used to fabricate quantum cascade detectors;[23] thus investigation of the electron transport of such heterostructures is required to further study properties such as the current–voltage characteristic and improve the performance of β-$(Al_xGa_{1-x})_2O_3$/Ga_2O_3 heterostructure-based devices. When applied to charge transport in semiconductors, the Monte Carlo (MC) method is much more flexible than the iterative method, and it can be used to model high-field electron transport in semiconductor materials.[24] To the best of our knowledge, the electron transport properties of unintentionally doped β-$(Al_xGa_{1-x})_2O_3$/Ga_2O_3 heterostructures have not yet been investigated by MC simulation, which stimulated us to investigate this and hope to fill the gap.

In this work, a systematic three-valley MC simulation of the steady-state and transient electron transport characteristics was carried out on β-$(Al_xGa_{1-x})_2O_3$/Ga_2O_3 heterostructures. Electronic band structures were determined by first-principles calculations. The wave function and energy eigenvalue were obtained by self-consistently solving the Schrödinger and Poisson equations. With five scattering mechanisms, the calculated mobility matches well with the reported experimental results, which verifies the correctness of our simulation.

2. Band structures and model description

In this study the β-$(Al_xGa_{1-x})_2O_3$ barrier and β-Ga_2O_3 well layers are nominally undoped and the electronic structure is investigated by a first-principles method based on density functional theory. Different Al mole fractions of β-$(Al_xGa_{1-x})_2O_3$ supercells can be constructed by replacing some Ga atoms by Al atoms in β-Ga_2O_3. All systems are calculated in reciprocal space. The plane-wave cutoff energy is 400 eV,[25] and a $2\times4\times4$ Monkhorst–Pack grid is set to ensure good convergence between the computed structures and energies. In the self-consistent field calculation the convergence precision of the energy charge is 1.0×10^{-5} eV/atom, the maximum displacement convergence criterion is 1.0×10^{-3} Å, the maximum force acting on each atom is 0.03 eV·Å^{-1} and the maximum stress is 0.05 GPa. To correct the band gap value of β-Ga_2O_3, the Hubbard U, an effective on-site Coulomb interaction scheme, is incorporated into the generalized gradient approximation method to improve the theoretical prediction, and the parameter U is set to be 14.0 eV for the Ga 3d orbital and 8.35 eV for the O 2p orbital.[26] Figure 1 presents the electronic band structure for pure β-Ga_2O_3 and β-$(Al_xGa_{1-x})_2O_3$ ($x=0.125$, 0.188, and 0.313). The corrected band gap and the fitted effective mass of the lowest valley are compared with the available experimental results (see Table 1). The good agreement between the simulated values and the experimental data[12,17,18,27,28] confirms the validity of our calculation. These results are used for the next self-consistent numerical calculations and MC simulation.

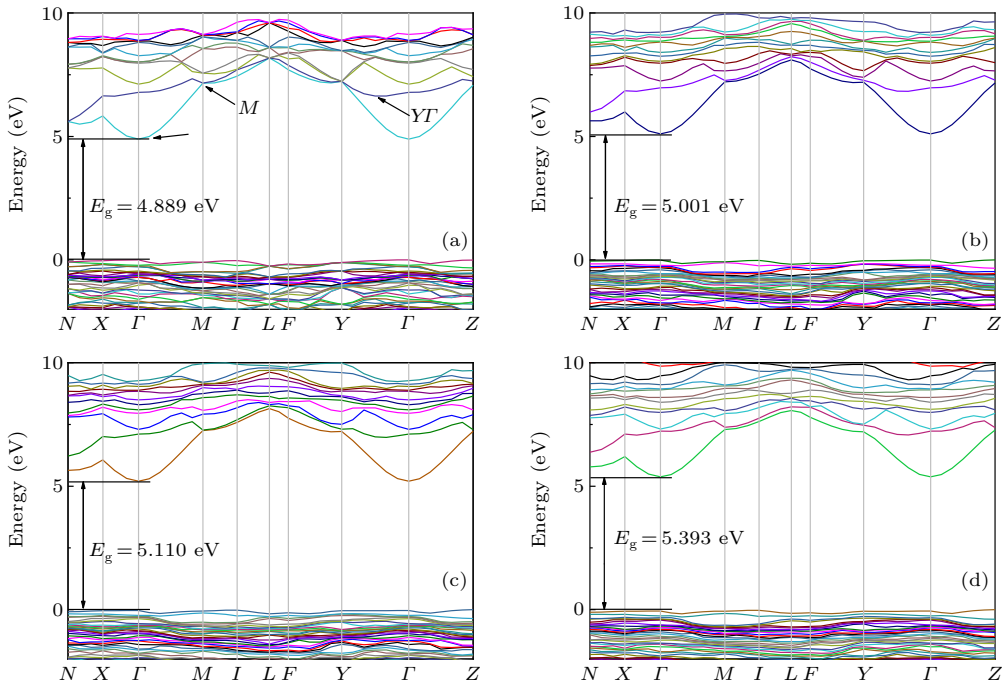


Fig. 1. Calculated electronic structures for (a) β-Ga_2O_3, (b) β-$(Al_{0.125}Ga_{0.875})_2O_3$, (c) β-$(Al_{0.188}Ga_{0.812})_2O_3$ and (d) β-$(Al_{0.313}Ga_{0.687})_2O_3$.

Table 1. Material parameters for β-$(Al_xGa_{1-x})_2O_3$.

Parameter (eV)/(m_0)	Simulated value	Experimental value
Band gap ($x=0$)	4.889	4.9[18]
Band gap ($x=0.125$)	5.001	4.96 ($x=0.12$)[27]
Band gap ($x=0.188$)	5.110	5.20 ($x=0.2$)[12]
Band gap ($x=0.313$)	5.393	5.32 ($x=0.31$)[27]
Effective mass ($x=0$) (Γ, $Y\Gamma$, M)	(0.274, 0.433, 0.642)	0.28 (lowest valley)[28]
Effective mass ($x=0.125$) (Γ, $Y\Gamma$, M)	(0.295, 0.585, 0.719)	0.294 (lowest valley)[17]
Effective mass ($x=0.188$) (Γ, $Y\Gamma$, M)	(0.306, 0.729, 0.849)	0.301 (lowest valley)[17]
Effective mass ($x=0.313$) (Γ, $Y\Gamma$, M)	(0.333, 0.858, 0.978)	0.313 (lowest valley)[17]

Table 2. Main material parameters.

Parameter	Value
Static dielectric constant	$10.2\varepsilon_0$[13]
High-frequency dielectric constant	$3.57\varepsilon_0$[13]
Mass density	5880 kg·m^{-3} [30]
Sound velocity	6880 m·s^{-1} [4]
Acoustic deformation potential	6.9 eV[4]
Polar optical phonon energy	48 meV[4,29]
Average roughness height	0.45 nm[13]
Horizontal correlation length	4.7 nm[13]
Dislocation density	10^5 cm^{-2} [10]

In our MC simulation, the critical features of the conduction bands are the Γ, $Y\Gamma$, and M valleys. The quantization effect is considered only in the Γ valley with the five lowest subbands. The material parameters[4,10,13,29,30] used in the calculations are listed in Table 2. To compute the scattering rates of the 2DEG, the energy levels and wave functions are achieved by self-consistently solving the Schrödinger–Poisson equations. The scattering mechanisms include interface roughness scattering (IRS), polar optical phonon scattering (POP), alloy disorder scattering (ADS), acoustic deformation potential scattering (ADP) and dislocation scattering (DIS). Then the total mobility can be obtained using Matthiesen's rule. The main processes of the calculation are described below.

Within the framework of the effective mass approximation, the Schrödinger equation can be written as

$$\left[-\frac{\hbar^2}{2m^*}\frac{\mathrm{d}^2}{\mathrm{d}z^2}+U(z)\right]\zeta_i(z)=E_i\zeta_i(z), \tag{1}$$

where $\hbar$ is the reduced Planck constant, m^* is the effective mass and $\zeta_i(z)$ is the wave function for the i-th subband in the β-$(Al_xGa_{1-x})_2O_3$/Ga_2O_3 quantum well with energy eigenvalue E_i. The potential energy $U(z)$ can be expressed as

$$U(z)=-e\phi(z)+\Delta E_{\mathrm{c}}(z), \tag{2}$$

where e is the electronic charge, $\phi(z)$ is the electrostatic potential and $\Delta E_{\mathrm{c}}(z)$ is the conduction band discontinuity at the β-$(Al_xGa_{1-x})_2O_3$/Ga_2O_3 interface.[31] Then, the Poisson equation is written as

$$\frac{\mathrm{d}}{\mathrm{d}z}\left[\varepsilon(z)\frac{\mathrm{d}\phi}{\mathrm{d}z}\right]=en(z), \tag{3}$$

where $\varepsilon(z)$ is the dielectric constant. The electron concentration $n(z)$ in the quantum well can be obtained as

$$n(z)=\sum_{i=1}^{m}|\zeta_i(z)|^2\frac{m^*k_{\mathrm{B}}T}{\pi\hbar^2}\ln\left[1+\exp\left(\frac{E_{\mathrm{F}}-E_i}{k_{\mathrm{B}}T}\right)\right]. \tag{4}$$

Here, m is the number of occupied subbands, k_{B} is the Boltzmann constant, T is the temperature and E_{F} is the Fermi level.

When manufacturing heterostructures the roughness of the interface between different materials cannot be completely avoided, thus the IRS must be considered. The inverse of the momentum relaxation time τ limited by IRS can be expressed by

$$\frac{1}{\tau_{\mathrm{IRS}}}=\frac{m^*\Delta^2\Lambda^2}{2\hbar^3}\exp\left(-\frac{\Lambda^2q^2}{4}\right)\times\int_0^{\pi}\left|\int\frac{\partial U}{\partial z}|\zeta_n(z)||\zeta_m(z)|\mathrm{d}z\right|^2S_{\mathrm{c}}(1-\cos\theta)\mathrm{d}\theta, \tag{5}$$

where Δ is the average roughness height, Λ is the horizontal correlation length, $q=2k\sin(\theta/2)$, k is the wave vector, θ is the angle between electron wave vectors before and after scattering, S_{c} is the screening factor, $S_{\mathrm{c}}=\left[\frac{q}{q+q_{\mathrm{s}}}\right]^2$, and $q_{\mathrm{s}}=\left[\frac{m^*e^2}{2\pi\varepsilon\hbar^2}\right]\int\zeta_n^2(z)\int\zeta_m^2(z')\exp(-q|z-z'|)\,\mathrm{d}z\mathrm{d}z'$.

As is known, POP plays an important role in limiting the room temperature electron mobility in β-$(Al_xGa_{1-x})_2O_3$/Ga_2O_3 heterostructures. The τ limited by POP can be given by

$$\frac{1}{\tau_{\mathrm{POP}}}=\frac{m_{\mathrm{e}}e^2E_{\mathrm{l}}\left(N_{\mathrm{q}}+(1/2)\pm(1/2)\right)}{2\hbar^2}\left(\frac{1}{\varepsilon_\infty}-\frac{1}{\varepsilon_{\mathrm{s}}}\right)\times\iint\zeta_n^*(z)\zeta_n(z')\zeta_m^*(z)\zeta_m(z')\mathrm{d}z\mathrm{d}z'\int_0^{2\pi}\mathrm{d}\theta\frac{\mathrm{e}^{-Q|z-z'|}}{Q} \tag{6}$$

with

$$Q=\left(k_{\mathrm{i}}^2+k_{\mathrm{f}}^2-2k_{\mathrm{i}}k_{\mathrm{f}}\cos\theta\right)^{1/2}, \tag{7}$$

$$k_{\mathrm{f}}^2=k_{\mathrm{i}}^2+\frac{2m^*}{\hbar}\left(E_{\mathrm{i}}-E_{\mathrm{f}}\pm E_{\mathrm{l}}\right). \tag{8}$$

Here, m_{e} is the effective mass of β-Ga_2O_3 and E_{l} is the polar optical photon energy, the value of which is based on the fitting of experimental data. In β-Ga_2O_3, although there are eight longitudinal optical phonon modes in a (100) direction, it can be found that a POP energy of 48 meV is good enough to capture the POP effect based on the Fröhlich model.[4,13] N_{q} is the phonon occupation number, ε_∞ is the high-frequency dielectric constant, ε_{s} is the static dielectric constant, k_{i} and k_{f} are the wave vectors of the initial and final states, respectively, '+' represents phonon absorption and '–' represents phonon emission.

3. Analysis and discussion

To investigate the electron transport properties of β-$(Al_xGa_{1-x})_2O_3/Ga_2O_3$, the mobility of this heterostructure is studied first and the microscopic behaviors such as electron velocity and electron occupancy then discussed to further understand the transport phenomena of β-$(Al_xGa_{1-x})_2O_3/Ga_2O_3$ and the corresponding mechanisms. Finally, on the basis of the obtained velocity and displacement of the electrons, the diffusion coefficient is studied. In this work, all the properties are discussed at different temperatures or electric field strengths.

As is known, mobility is an important parameter for semiconductor devices such as transistors because it determines the power dissipation and switching speed.[32] To simulate the mobility properties of β-$(Al_xGa_{1-x})_2O_3/Ga_2O_3$, some key parameters of the conduction band are required. The calculated conduction band profile, the first subband energy level and the corresponding wave function for β-$(Al_{0.188}Ga_{0.812})_2O_3/Ga_2O_3$ are demonstrated in Fig. 2(a). Confinement of the 2DEG at the interface leads to the formation of energy subbands because of the quantization of the electronic band structure.[21] The ground wave function is well localized with some penetration to the potential barrier due to the finite conduction band offsets, which may induce ADS. The variation of the calculated electron mobility in a β-$(Al_{0.188}Ga_{0.812})_2O_3/Ga_2O_3$ heterostructure with temperature is displayed in Fig. 2(b). The reported theoretical and experimental results[13,15,16,19] are also provided for comparison. As can be observed, when IRS, POP and ADP are separately considered, the corresponding electron mobility calculated is in accordance with the reported theoretical result. When all five different scattering mechanisms are included, the calculated 2DEG electron mobility (the solid green line in Fig. 2(b)) matches well with the experimental data at 100 K–300 K. However, at low temperatures the calculated mobility is higher than that in the experiment, mainly because the remote impurity scattering (RI) and background impurity scattering (BI) have a great impact on the doped heterostructures in the experiment. This effect is negligible for the unintentionally doped heterostructure in our model; therefore, when the contributions of RI and BI are removed, the calculated electron mobility is in good agreement with the experimental data, thus confirming the validity of our model. Figures 2(c) and 2(d) illustrate the electron mobility of β-$(Al_xGa_{1-x})_2O_3/Ga_2O_3$ with different Al compositions versus the applied electric field by MC simulation at different temperatures. In Fig. 2(c), the mobility decreases with the increase in the temperature for a fixed electric field, and the mobility for 10 kV·cm^{-1} at 300 K is approximately 153.669 cm^2·V^{-1}·s^{-1}. This is because the

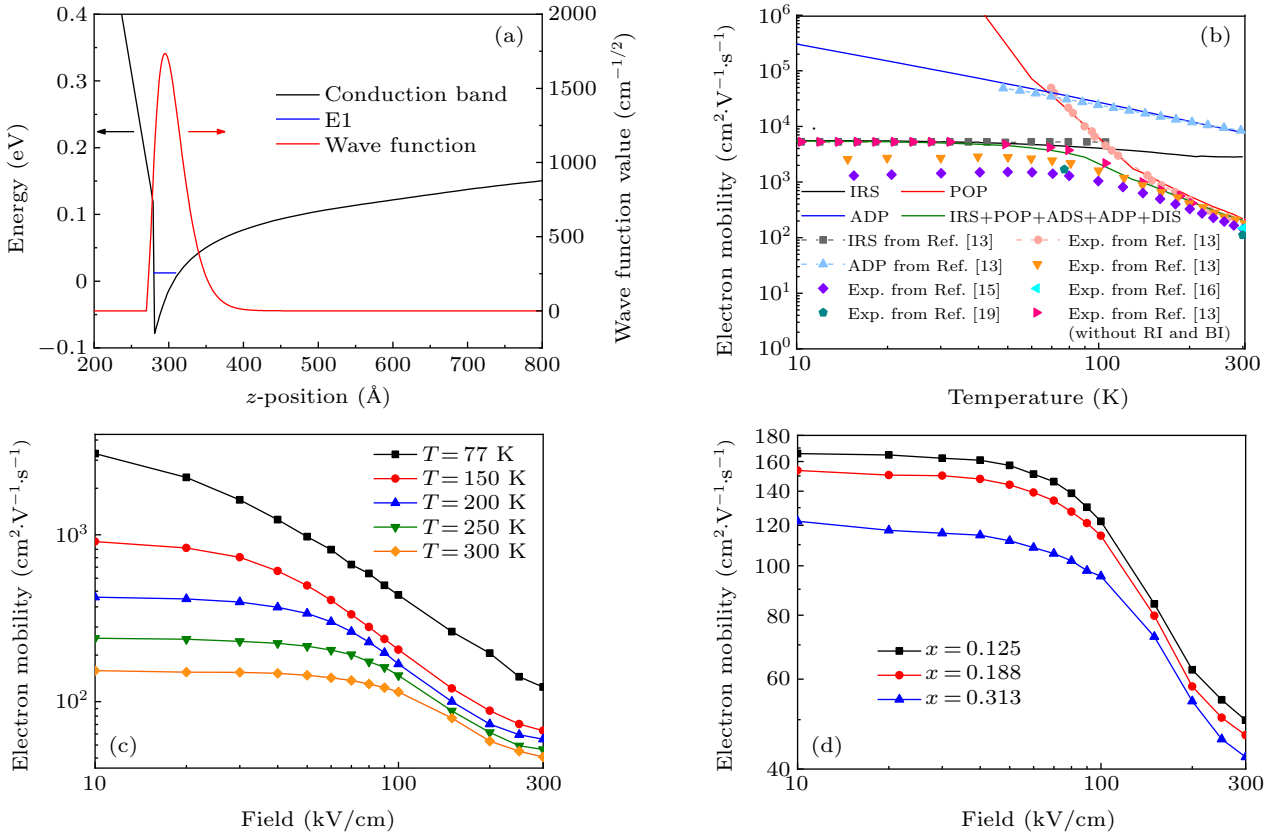


Fig. 2. (a) Calculated energy band profile, ground state subband energy level and the corresponding wave function of a β-$(Al_{0.188}Ga_{0.812})_2O_3/Ga_2O_3$ quantum well at 300 K. (b) β-$(Al_{0.188}Ga_{0.812})_2O_3/Ga_2O_3$ low-field electron mobility as a function of temperature. The solid lines and dashed lines with symbols represent the theoretical data, and the scatter dots denote the experimental data. Electron mobility as a function of the applied electric field in (c) β-$(Al_{0.188}Ga_{0.812})_2O_3/Ga_2O_3$ at different temperatures and (d) β-$(Al_xGa_{1-x})_2O_3/Ga_2O_3$ with different Al compositions at 300 K.

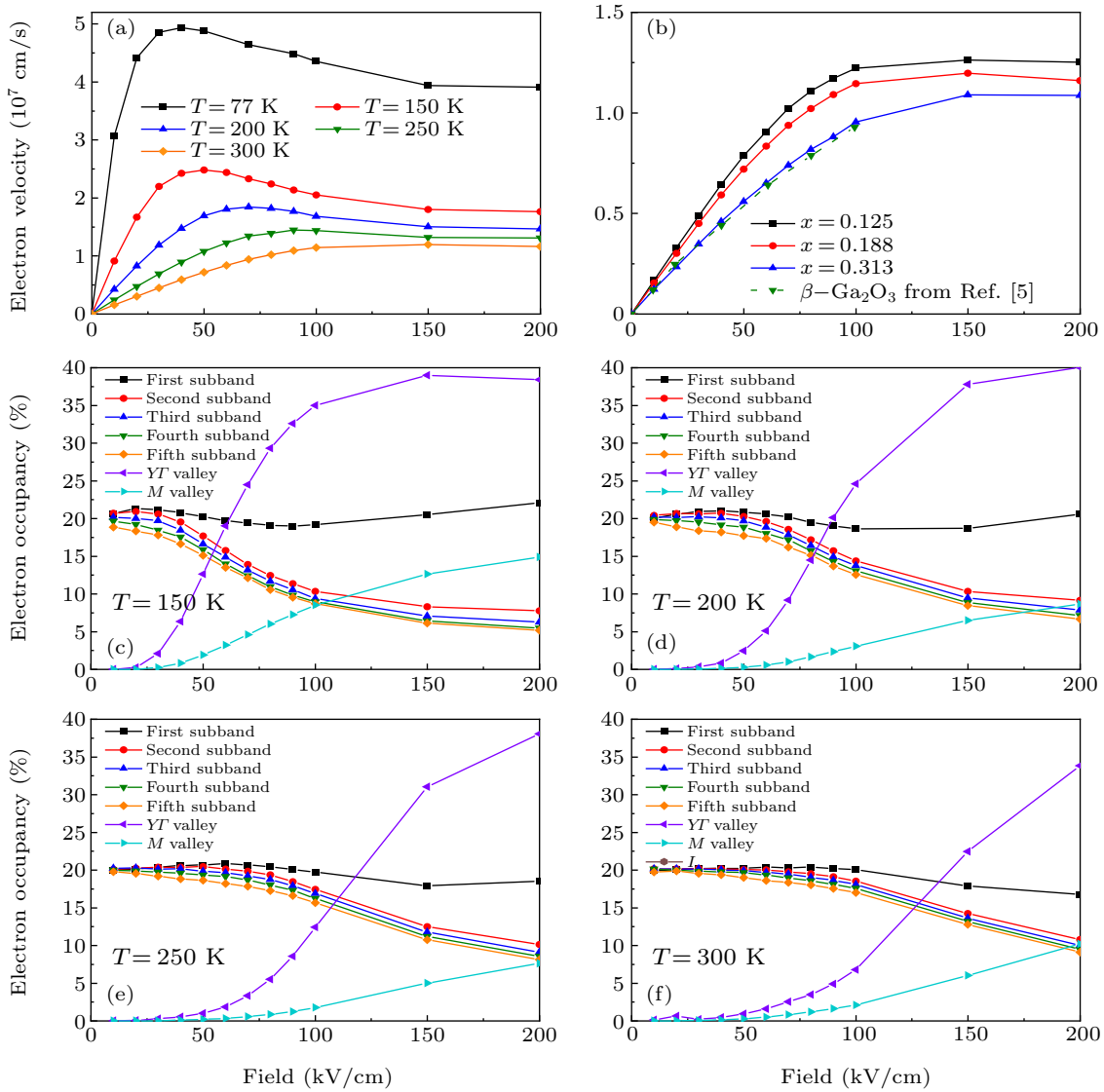


Fig. 3. Electron steady-state drift velocity as a function of the applied electric field in (a) β-$(Al_{0.188}Ga_{0.812})_2O_3/Ga_2O_3$ at different temperatures, and (b) β-$(Al_xGa_{1-x})_2O_3/Ga_2O_3$ with varying Al compositions at 300 K. The dashed lines with symbols represent the steady-state drift velocity of β-Ga_2O_3. (c)–(f) Electrons' occupancy as a function of the applied electric field in β-$(Al_{0.188}Ga_{0.812})_2O_3/Ga_2O_3$ at different temperatures.

total scattering rate increases with increasing temperature. The electron mobility at room temperature decreases with the increasing Al composition when the electric field remains constant in Fig. 2(d), which is due to the fact that the impacts of ADS, DIS, and IRS are strengthened by the increasing Al content.[33]

To gain a good understanding of the electron mobility characteristic of β-$(Al_xGa_{1-x})_2O_3/Ga_2O_3$ heterostructures, the microscopic behavior of the electrons must be investigated in depth. As is known, steady-state electron transport is the dominant transport mechanism in devices with larger dimensions. For devices with smaller dimensions, however, transient electron transport must also be considered when evaluating device performance. Therefore, both the electron steady-state drift velocity and the electron transient velocity of β-$(Al_xGa_{1-x})_2O_3/Ga_2O_3$ were investigated in this work.

The electron drift velocity versus electric field of β-$(Al_xGa_{1-x})_2O_3/Ga_2O_3$ heterostructures is shown in Figs. 3(a) and 3(b). In Fig. 3(a), both the peak and the saturation velocities are dependent on temperature. This is because the POP rate increases significantly with increasing temperature. Besides, at a fixed temperature, the dependence of the drift velocity on electric field is almost linear at low electric fields. After the electron drift velocity reaches its peak value, the velocity decreases in response to further increase in the applied electric field. This behavior is a clear evidence of negative differential mobility (NDM). NDM occurs because electrons in the Γ valley will accelerate under high fields and gain enough energy to transfer to the satellite valleys. As can be seen in the electron occupancy curves in Figs. 3(c)–3(f), the inter-valley deformation scattering becomes effective when the electrons significantly populate the satellite valleys, and the effective masses of the satellite valleys are higher than that of the Γ valley. Then, with a continued increase in electric field, the short-range intra-valley electron–phonon interaction would result in saturation of the velocity.[34] Specif-

ically, at 300 K with an electric field of 150 kV·cm^{-1}, the maximum drift velocity is 1.197×10^7 cm·s^{-1}. This implies that β-$(Al_xGa_{1-x})_2O_3/Ga_2O_3$ can tolerate a high voltage with steady performance. Figure 3(b) gives the electron drift velocity versus electric field of β-Ga_2O_3 for comparison. As can be observed, when the electric field is within 100 kV·cm^{-1}, the steady-state drift velocities of both β-Ga_2O_3 and β-$(Al_xGa_{1-x})_2O_3/Ga_2O_3$ increase almost linearly with increasing electric field. The average drift velocity decreases with the increasing Al content. This situation is due to the increase in 2DEG density induced by the increasing Al content: an increasing number of electrons are electrostatically pushed closer to the heterointerface and the impact of IRS will be enhanced.

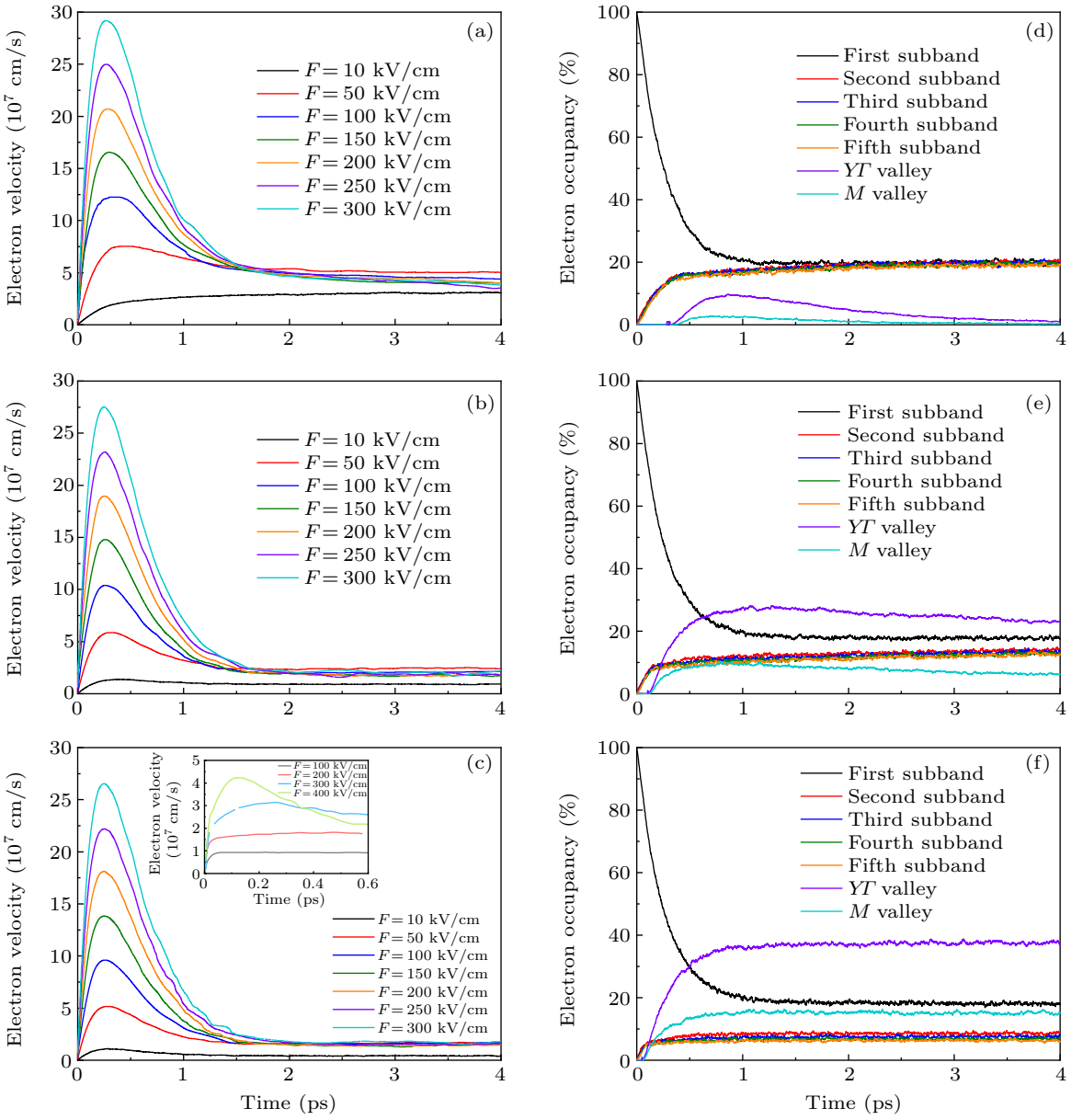


Fig. 4. Transient electron velocity as a function of the applied electric field in β-$(Al_{0.188}Ga_{0.812})_2O_3/Ga_2O_3$ at (a) 77 K, (b) 150 K, and (c) 300 K. Inset: the transient electron velocity of β-Ga_2O_3 (results from Ref. [5]). The electron occupancy of β-$(Al_{0.188}Ga_{0.812})_2O_3/Ga_2O_3$ as a function of time at 300 K with an applied electric field of (d) 50 kV·cm^{-1}, (e) 150 kV·cm^{-1}, and (f) 300 kV·cm^{-1}.

The electron transient characteristics of β-$(Al_{0188}Ga_{0.812})_2O_3/Ga_2O_3$ heterostructure are presented in Fig. 4. Figures 4(a)–4(c) show the transient electron velocity versus the applied electric field at different temperatures. In the inset of Fig. 4(c) the electron transient velocity versus time for β-Ga_2O_3 is given for comparison. As can be seen, the critical electric fields corresponding to the significant overshoot of β-$(Al_xGa_{1-x})_2O_3/Ga_2O_3$ and β-Ga_2O_3 are 100 kV·cm^{-1} and 300 kV·cm^{-1}, respectively. Besides, for the same electric field the peak transient velocities of β-Ga_2O_3 are lower than those of β-$(Al_xGa_{1-x})_2O_3/Ga_2O_3$. The overshoot is mainly because the momentum relaxation time is much lower than the energy relaxation time, and the time required for the transient process is of the same order of magnitude as the energy relaxation time. It can also be observed that the peak transient velocities are much higher than the peak velocities of elec-

tron steady-state drift properties in Fig. 3(a) under the same conditions. This is because in the ballistic regime the electrons can acquire energy from the applied field without losing energy to the lattice from scattering, and their velocity will reach a higher value than in the steady state.[35] Figures 4(d)–4(f) show the time evolution of the electron occupancy in β-$(Al_{0.188}Ga_{0.812})_2O_3/Ga_2O_3$ at 300 K for different electric fields. It can be seen that the population of electrons in the first subband decreases at the beginning and that in higher subbands gradually increases. However, most electrons are still in the Γ valley, therefore the drift velocity initially increases, as shown in Fig. 4(c). As time progresses, electron excitation to the higher subbands and valleys begins to dominate, causing a decrease in the drift velocity. This phenomenon has also been observed in MgZnO/ZnO heterostructures by MC simulation.[33]

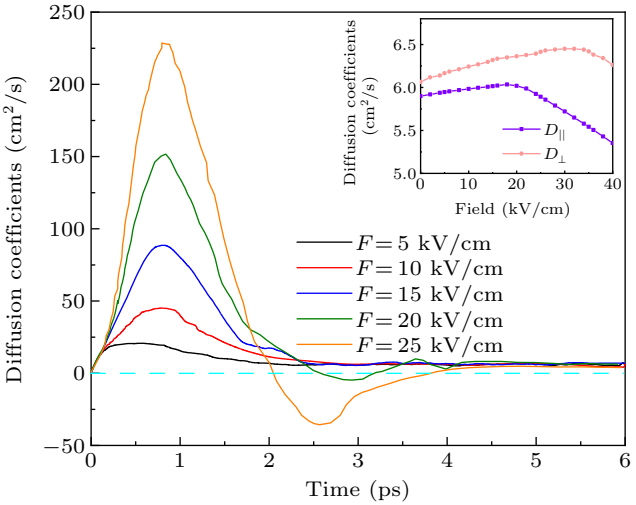


Fig. 5. Longitudinal diffusion coefficients as a function of time for β-$(Al_{0.188}Ga_{0.812})_2O_3/Ga_2O_3$ at 300 K for different applied electric fields. Inset: longitudinal and transverse diffusion coefficients as a function of the applied electric field for β-$(Al_{0.188}Ga_{0.812})_2O_3/Ga_2O_3$ at 300 K.

It is known that diffusion arises from the correlation between the velocity and displacement of particles, and the diffusion coefficient is of great significance in the study of the effect of carrier diffusion on the microwave characteristics of integrated β-$(Al_xGa_{1-x})_2O_3/Ga_2O_3$ devices.[36] Figure 5 presents the longitudinal diffusion coefficient ($D_{\parallel}$) versus time for different electric fields at room temperature. As can be seen, $D_{\parallel}$ sharply increases within the first 1 ps, then decreases with time and finally approaches zero. Because the diffusion coefficient is related to the correlation function of the velocity fluctuation for electrons,[36] and the transient electron velocity V_t will lose its correlation with $V_t = 0$ with time due to the irregular fluctuations of the velocity in β-$(Al_{0.188}Ga_{0.812})_2O_3/Ga_2O_3$. The inset shows $D_{\parallel}$ and the transverse diffusion coefficient ($D_{\perp}$) versus electric field for β-$(Al_{0.188}Ga_{0.812})_2O_3/Ga_2O_3$ at 300 K. $D_{\parallel} < D_{\perp}$ in the whole range of electric field is caused by the anisotropic effect of the crystallographic orientation.[37] This phenomenon is a significant feature of multivalley semiconductors[36] and can also be found in GaAs by MC investigation.[38]

4. Conclusion

In summary, a three-valley ensemble MC simulation is presented for detailed investigation of the electron transport characteristics of β-$(Al_xGa_{1-x})_2O_3/Ga_2O_3$ heterostructures. The electronic band structures are obtained by first-principles calculations, and the results are important parameters used in our simulations. Considering the quantization effects in the Γ valley, the wave functions and energy levels are obtained by iterative calculation and then used to compute the scattering rates of the 2DEG. The achieved electron mobility matches well with the experimental data, therefore proving the validity of our models. For β-$(Al_xGa_{1-x})_2O_3/Ga_2O_3$, the electron mobility decreases when the Al content increases for a fixed electric field. A region of negative differential mobility can be observed in the velocity–field characteristics. At room temperature, the steady-state electron velocity could reach the order of 10^7 cm·s^{-1} at 150 kV·cm^{-1}. Furthermore, a pronounced anisotropy of the diffusion coefficient is found. This work provides detailed information regarding the transport properties of β-$(Al_xGa_{1-x})_2O_3/Ga_2O_3$, which is essential knowledge that will benefit the design and fabrication of high-quality β-$(Al_xGa_{1-x})_2O_3/Ga_2O_3$ heterostructure-based devices.

Acknowledgments

Project supported by the National Natural Science Foundation of China (Grant No. 61474090), the Key Research and Development Program of Shaanxi Province of China (Grant No. 2017ZDXM-GY-052), and the Fundamental Research Funds for the Central Universities (Grant No. 20109205456), and the Innovation Fund of Xidian University.

References

[1] Sun W M, Sun B Y, Li Shan, Ma G L, Gao A, Jiang W Y, Zhang M L, Li P G, Liu Z and Tang W H 2022 *Chin. Phys. B* **31** 024205
[2] Qian L X, Gu Z, Huang X, Liu H, Lv Y, Feng Z and Zhang W 2021 *ACS Appl. Mater. Interfaces* **13** 40837
[3] Nishinaka H, Nagaoka T, Kajita Y and Yoshimoto M 2021 *Mater. Sci. Semicond. Process.* **128** 105732
[4] Bauman D A, Panov D I, Zakgeim D A, Spiridonov V A, Kremleva A V, Petrenko A A, Smirnov A M, Odnoblyudov M A, Bougrov V E and Romanov A E 2021 *Phys. Status Solidi A* **218** 2100335
[5] Zhang Z C, Wu Y, Lu C and Ahmed S S 2018 13*th IEEE Nanotechnol. Mater. Devices Conf.* October 14–17, 2018 Portland Or United States pp. 1–4
[6] Fares C, Ren F, Hays D C, Gila B P, Tadjer M, Hobart K D and Pearton S J 2018 *Appl. Phys. Lett.* **113** 182101
[7] Ghadi H, McGlone J F, Feng Z, Bhuiyan A F, Zhang Y, Zhao H, Armstrong A, Burns G R, Vizkelethy G, Bielejec E, Arehart A R and Ringel S A 2021 *Oxide-based Materials and Devices XII*, March 6–11, 2021 United States, pp. 31–37

[8] Vaidya A, Sarker J, Zhang Y, Lubecki L, Wallace J, Poplawsky J D, Sasaki K, Kuramata A, Goyal A, Gardella J A, Mazumder B and Singisetti U 2019 *J. Appl. Phys.* **126** 095702

[9] Lyman J E and Krishnamoorthy S 2020 *J. Appl. Phys.* **127** 173102

[10] Kaun S W, Wu F and Speck J S 2015 *J. Vac. Sci. Technol. A* **33** 041508

[11] Patnaik A, Jaiswal N K, Singh R and Sharma P 2022 *Semicond. Sci. Technol.* **37** 025002

[12] Krishnamoorthy S, Xia Z, Joishi C, Zhang Y, McGlone J, Johnson J, Brenner M, Arehart A R, Hwang J, Lodha S and Rajan S 2017 *Appl. Phys. Lett.* **111** 023502

[13] Zhang Y, Neal A, Xia Z, Joishi C, Johnson J M, Zheng Y, Bajaj S, Brenner M, Dorsey D, Chabak K, Jessen G, Hwang J, Mou S, Heremans J P and Rajan S 2018 *Appl. Phys. Lett.* **112** 173502

[14] Zhang Y, Joishi C, Xia Z, Benner M, Lodha S and Rajan S 2018 *Appl. Phys. Lett.* **112** 233503

[15] Zhang Y, Xia Z, McGlone J, Sun W, Joishi C, Arehart A R, Ringel S A and Rajan S 2019 *IEEE Trans. Electron Devices* **66** 1574

[16] Kalarickal N K, Xia Z, McGlone J F, Liu Y, Moore W, Arehart A R, Ringel S A and Rajan S 2020 *J. Appl. Phys.* **127** 215706

[17] Ranga P, Rishinaramangalam A, Varley J, Bhattacharyya A, Feezell D and Krishnamoorthy S 2019 *Appl. Phys. Express* **12** 111004

[18] Vogt P, Mauze A, Wu F, Bonef B and Speck J S 2018 *Appl. Phys. Express* **11** 115503

[19] Ranga P, Bhattacharyya A, Chmielewski A, Roy S, Sun R, Scarpulla M A, Alem N and Krishnamoorthy S 2021 *Appl. Phys. Express* **14** 025501

[20] Ghosha K and Singisetti U 2017 *J. Mater. Res.* **32** 4142

[21] Kumar A, Ghosha K and Singisetti U 2020 *J. Appl. Phys.* **128** 105703

[22] Hamaguchi C, Miyatsuji K and Tanimoto H 1986 *High-Speed Electronics* (Vol. 22) (Berlin, Heidelberg: Springer) pp. 112–115

[23] He J, Wang P, Chen H, Guo X, Guo L and Yang Y 2017 *Appl. Phys. Express* **10** 011101

[24] Jacoboni C and Reggiani L 1983 *Rev. Mod. Phys.* **55** 645

[25] Peelaers H and Walle C G V 2015 *Phys. Status Solidi B Basic Res.* **252** 828

[26] Liu J, Gao S, Li W, Dai J, Suo Z and Suo Z 2022 *Cryst. Res. Technol.* **57** 2100126

[27] Xiao H, Shao G, Sai Q, Xia C, Zhou S and Yi X 2016 *J. Inorg. Mater.* **31** 1258

[28] Mohamed M, Janowitz C, Unger I, Manzke R, Galazka Z, Uecker R, Fornari R, Weber J R, Varley J B and Walle C G V 2010 *Appl. Phys. Lett.* **97** 211903

[29] Ma N, Tanen N, Verma A, Guo Z, Luo T F, Xing H L and Jena D 2016 *Appl. Phys. Lett.* **109** 212101

[30] Ghosh K and Singisetti U 2019 *Gallium Oxide* (1st edn.) (Netherlands: Elsevier) pp. 149–168

[31] Peelaers H, Varley J B, Speck J S and Walle C G 2018 *Appl. Phys. Lett.* **112** 242101

[32] Jena D and Konar A 2007 *Phys. Rev. Lett.* **98** 136805

[33] Chen H Y, Wang P, Cheng J S, Li Z L, Guo L X and Zhang Z Y 2017 *IEEE Trans. Electron Devices* **64** 2148

[34] Ghosh K and Singisetti U 2017 *J. Appl. Phys.* **122** 035702

[35] Ng K K 2009 *Complete Guide to Semiconductor Devices* (2nd edn.) (Piscataway: IEEE Press) pp. 595–646

[36] Fauquembergue R, Zimmermann J, Kaszynski A, Constant E and Micoundes G 1980 *J. Appl. Phys.* **51** 1065

[37] Brunetti R, Jacoboni C, Nava F, Reggiani L, Bosman G and Zijlstra R J J 1981 *J. Appl. Phys.* **52** 6713

[38] Fauquembergue R, Zimmermann J, Kaszynski A, Constant E and Micoundes G 1980 *J. Appl. Phys.* **51** 1065